Research Article

Mohammed S. Algahtani, Rabbani Syed*, Mudassar Shahid, Mohd Abul Kalam, Mukesh Goel, and R. Lakshmipathy*

Clerodendron phlomoides leaf extract-mediated synthesis of selenium nanoparticles for multiapplications

https://doi.org/10.1515/gps-2025-0027 received February 04, 2025; accepted May 12, 2025

Abstract: This study aimed at the green synthesis of selenium nanoparticles (SeNPs) using an aqueous extract of Clerodendron phlomoides leaves as both reducing and stabilizing agents. The success of SeNP synthesis was confirmed using various analytical characterization techniques such as UV-Vis, FTIR, XRD, SEM, and TEM techniques. The surface plasmon resonance (SPR) of SeNPs was observed at 325 nm, confirming their polycrystalline nature, while FTIR analysis revealed the presence of flavonoids on the surface of SeNPs that acted as reducing and stabilizing agents for nanoparticle formation. The crystalline pattern obtained from XRD revealed primitive hexagonal structures of SeNPs. The spherical-shaped SeNPs, with a size of around 30 nm, were visualized and confirmed through SEM and TEM investigations. A good antiproliferative activity against the HepG-2 cell line at 13 µg·mL⁻¹ and a significant improvement in SOD activity demonstrated the ability of flavonoid-capped SeNPs to act as potent anticancer and antioxidant agents. SeNPs also exhibited excellent antimicrobial activity against Escherichia coli, Pseudomonas aeruginosa, and Staphylococcus aureus strains by disrupting the cell membranes. Further, an RSM-based investigation on the removal of Pb²⁺ ions showed superior adsorption efficiency of SeNPs, with a loading capacity of 101.9 mg·g⁻¹. The results of

this study demonstrate the multi-application potential of SeNPs synthesized through green principles using leaf aqueous extract of Clerodendron phlomoides.

Keywords: selenium nanoparticles, green synthesis, *Clerodendron* phlomoides, adsorption, MTT assay and antimicrobial

1 Introduction

Selenium (Se) is a potential nanomaterial for drug delivery and anticancer applications due to its antiproliferative, antioxidant, chemopreventive, and chemotherapeutic properties, as well as its high bioavailability at injury sites [1-3]. Numerous diseases, such as Parkinson's disease, Kashin-Beck's disease, cognitive impairment, seizures, and Alzheimer's disease [4], are associated with Se deficiency. Additionally, the incidence of thyroid [5] and gastrointestinal disorders increases with insufficient Se levels. Selenium nanoparticles (SeNPs) exhibit superior free radical scavenging activity, which depends on their size [6]. They also demonstrate strong antiproliferative effects against breast, brain, kidney, lung, and osteosarcoma cancers, making them promising candidates for next-generation chemopreventive and chemotherapeutic agents. Furthermore, SeNPs possess unique physical properties, including piezoelectricity, photoconductivity, excellent photoelectrical and optical properties, and fair catalytic activity, making them highly versatile for various applications [7,8].

SeNPs can be synthesized through various methods, including solvothermal/hydrothermal, electrochemical, chemical reduction, sonochemical, and laser ablation techniques [9,10]. While these methods are effective in producing SeNPs, they often require toxic chemicals, extreme reaction conditions, or generate harmful by-products. In contrast, green synthesis using plant extracts offers an eco-friendly and sustainable alternative, eliminating the need for hazardous reagents and avoiding toxic by-product

Mohammed S. Alqahtani, Mudassar Shahid, Mohd Abul Kalam: Department of Pharmaceutics, College of Pharmacy, King Saud University, P.O. Box 2457, Riyadh, 11451, Saudi Arabia Mukesh Goel: Department of Engineering and Maths, College of

Business, Technology and Engineering, Sheffield Hallam University, Sheffield, United Kingdom

^{*} Corresponding author: Rabbani Syed, Department of Pharmaceutics, College of Pharmacy, King Saud University, P.O. Box 2457, Riyadh, 11451, Saudi Arabia, e-mail: rsyed@ksu.edu.sa

^{*} Corresponding author: R. Lakshmipathy, Directorate of Learning and Development, SRM Institute of Science and Technology, Kattankulathur, Tamilnadu, 603203, India, e-mail: lakshmipathy.vit@gmail.com

formation [11]. The phytochemicals present in plant extracts, such as proteins, polyphenols, flavonoids, polysaccharides, terpenoids, and other organic molecules, play a pivotal role in the reduction, stabilization, and fabrication of SeNPs. These bioactive compounds not only facilitate nanoparticle formation but also enhance their biocompatibility and functional properties.

Various plant extracts have been explored for the green synthesis of SeNPs, demonstrating their versatile applications across multiple domains [12,13]. For instance, SeNPs synthesized using Withania somnifera leaf extract (45–90 nm, spherical) exhibited photocatalytic degradation of methylene blue dye alongside antimicrobial activity against three bacterial strains [14]. Similarly, amorphous SeNPs (20–50 nm) produced from *Ulva fasciata* aqueous extract showed cytotoxic, apoptotic, and necrotic effects, as well as antibacterial activity against Gram-positive and Gram-negative strains [15]. Further studies utilized Cassia javanica flower extract to synthesize spherical SeNPs (35-100 nm), which demonstrated antimicrobial properties and enhanced agricultural seed growth [16]. In an innovative approach, bimetallic Zn-Se nanoparticles fabricated using Gracilaria corticata extract displayed broad-spectrum antibacterial, anticancer, and antioxidant activities [17]. Additionally, SeNPs derived from Psidium guajava exhibited exceptional adsorption capacity (62.7 mg·L⁻¹) for Sb(III) ions, achieving 100% removal efficiency in real wastewater treatment [18]. Although the existing literature highlights the successful synthesis and diverse applications of SeNPs (antimicrobial, antioxidant, anticancer, and adsorbent), most studies focus on single functionalities. This underscores the need for comprehensive evaluation of plant-derived SeNPs for multi-application potential, enhancing their versatility in biomedical and environmental fields.

Clerodendron phlomoides is a medicinal plant with a long history of use in Indian and Chinese traditional medicine for treating diabetes, inflammation, and digestive disorders [19]. The plant is rich in diverse phytochemicals, which contribute to its broad therapeutic properties [20,21]. The presence of these bioactive molecules makes C. phlomoides leaves an excellent candidate for the biogenic synthesis of nanoparticles, as the surface-bound phytochemicals can enhance their biomedical efficacy. Despite its medicinal significance, there are no reported studies on the synthesis of elemental nanoparticles using C. phlomoides. To address this gap, we selected aqueous leaf extracts of *C. phlomoides* for the green synthesis of SeNPs in this study. The synthesized SeNPs were comprehensively evaluated for their antibacterial activity, anticancer potential, and adsorption capacity, demonstrating their multifunctional applications in biomedicine and environmental remediation.

2 Materials and methods

2.1 Chemicals

Sodium selenite, lead nitrate, sodium hydroxide, and hydrochloric acid were obtained from Sigma Aldrich. Malondialdehyde (MDA), tetrazolium salt, thiobarbituric acid, and hydrogen peroxide were sourced from Hi-Media Chemicals. Glutathione (GSH) was purchased from S.D. Fine Chemicals. Ampicillin was sourced from E-Merck Chemicals (USA). All chemicals were of analytical grade with 99.9% purity. Distilled water was used for all adsorption experiments.

2.2 Preparation of plant extracts

Fresh Clerodendron phlomoides leaves were collected from the local region and sun-dried for four consecutive days to remove complete moisture. The dried leaves were then mechanically ground into fine particles using a mortar and pestle. For aqueous extraction, $10\,\mathrm{g}$ of the powdered leaf material was immersed in $200\,\mathrm{mL}$ of distilled water and allowed to soak overnight at room temperature (25 \pm 2°C). The mixture was subsequently heated to $70\,\mathrm{°C}$ and maintained at this temperature for $20\,\mathrm{min}$ with constant stirring. After cooling to ambient temperature, the extract was filtered through Whatman No. 1 filter paper to remove particulate matter. The resulting clear filtrate was stored in sterile containers at $4\,\mathrm{°C}$ until further use in nanoparticle synthesis experiments.

2.3 Synthesis of SeNPs

An aliquot of 10 mL of aqueous extract of *Clerodendron phlomoides* was added to 100 mL of 3 mM sodium selenite solution. The synthesis was initiated by dropwise addition of the yellowish aqueous leaf extract to a 0.1 M sodium selenite solution (white-colored) under constant magnetic stirring at 500 rpm. An immediate color transition from white to yellow was observed upon the complete addition of the phytochemical extract. The reaction mixture was maintained at 80°C with continuous stirring, where the formation of a yellowish-white turbid suspension became

evident within 10 min. Notably, after 30 min of reaction time, the solution developed a distinct red coloration, confirming the successful reduction of selenite ions and nucleation of SeNPs. This rapid color transformation at elevated temperature (80°C) demonstrated the temperature-dependent kinetics of nanoparticle formation. Biogenic SeNPs were subsequently purified by centrifugation at 12,000 rpm for 15 min. The collected pellet underwent three washing cycles with deionized water to remove residual reactants and organic impurities. Final purification was achieved by oven-drying the nanoparticles at 60°C for 120 min. The resulting dried SeNPs were stored in amber vials for subsequent characterization and application studies.

2.4 Characterization of SeNPs

The optical and surface plasmon resonance (SPR) of SeNPs were evaluated using a Hitachi U-2800 Double-beam UVvisible spectrophotometer, and an investigation was performed in the range of 200-800 nm. The pure SeNPs and coated by the secondary metabolites were investigated by FTIR spectroscopy. An FTIR analysis (RX1-Perkin Elmer) in the 4,000-400 cm⁻¹ range was performed to identify the functional groups responsible for this reduction. Next, the morphology and shape of the SeNPs were examined using scanning electron microscopy (SEM; JEOL JSM IT1800). A small amount of SeNPs was spread on carbon tape adhered to a metallic stub. After removing loose particles with nitrogen gas, the sample was imaged in secondary electron mode at a 5 µm scale using the SEM instrument. Further, transmission electron microscopy (TEM; JEM 2100 plus, JEOL, Japan) was employed to further analyze the size and shape of the SeNPs. A drop of the SeNP suspension was dried on a copper grid before capturing TEM micrographs for detailed size and shape analysis. Utilizing monochromatic Cu K radiation ($\lambda = 1.5406$) operated at 40 kV and 30 mA at a 2θ angle pattern and scanning in the range of 20-80°, XPERT-PRO was utilized to evaluate the crystalline state of biosynthesized SeNPs. With the help of the JCPDS library, the gathered data were examined/ verified to consider the crystalline structure of the SeNPs.

2.5 MTT assay

MTT assay was implemented to evaluate the metabolic performance of cancerous cells through cell viability, growth, and cytotoxicity as indicators. It is a colorimetric assay based on the reduction of a yellow tetrazolium salt (3-(4,5-dimethylthiazol-2-yl)-2,5-diphenyltetrazolium bromide or MTT) into purple formazan crystals via cell metabolism. HepG2 cells, a human hepatoma cell line commonly used for drug metabolism and hepatotoxicity studies, were seeded at a density of 1×10^4 cells per well in 96-well plates and allowed to adhere overnight. The cells were then treated with green-synthesized SeNPs at various concentrations and incubated for 24 h at 37°C in a humidified atmosphere with 5% CO_2 . Following treatment, 20 μL of MTT solution (5 mg·mL⁻¹ in PBS) was added to each well, resulting in a final concentration of 0.5 mg·mL⁻¹. The color of MMT was yellow, and a tetrazole was reduced into a formazan compound with a purple color. The absorbance of the colored solution was evaluated at 570 nm using a spectrophotometer. The number of viable cells was evaluated.

2.6 Assessment of anti-oxidative enzyme activities and lipid peroxidation

Lipid peroxidation measurement: MDA levels were determined using a modified thiobarbituric acid reactive substance (TBARS) method [22]. This involved heating cell lysates with thiobarbituric acid and measuring the absorbance of the formed adduct at 532 nm, providing quantification of lipid peroxidation.

Catalase (CAT) activity assay: CAT enzyme activity was quantified by determining the rate of hydrogen peroxide decomposition using the method described by Aebi [23]. The reduction in absorbance at 240 nm was monitored spectrophotometrically, and enzyme activity expressed in units per milligram of protein.

GSH quantification: Total GSH was assessed using a colorimetric approach where reduced GSH converts a chromogenic reagent to a colored product measurable at 412 nm using the method developed by Moron et al. [24]. This method leverages the GSH reductase enzyme for the recycling of oxidized to reduced GSH.

Superoxide dismutase (SOD) activity: The activity of SOD was measured by its capacity to inhibit the reduction of nitroblue tetrazolium by superoxide radicals, with a decrease in absorbance recorded at 560 nm. This indicates the enzyme's efficacy in dismutating superoxide radicals into less reactive molecular species.

Protein concentrations were normalized using the Bradford protein assay, ensuring consistent reporting of enzyme activities. All measurements were replicated three times to ensure accuracy, with results presented as mean ± standard deviation.

2.7 Bacterial strains and culture protocols

Our study assessed the antibacterial effects of SeNPs on four distinct bacterial strains: Staphylococcus aureus (ATCC 25923), Escherichia coli (ATCC 25922), Pseudomonas aeruginosa (ATCC 27853), and Proteus vulgaris (ATCC 13315). These strains were cultured in Luria–Bertani (LB) broth at 37°C for 18–24 h until they reached the logarithmic phase of growth. Prior to each experimental run, fresh cultures were prepared overnight. The inocula were standardized to a density of approximately 1×10^6 CFU·mL $^{-1}$ using a sterile saline solution (0.85% NaCl) and adjusted to match the 0.5 McFarland standard using a spectrophotometer for consistency.

2.8 Antimicrobial testing methodology

The antibacterial activity was evaluated using the agar well diffusion technique. Mueller–Hinton agar plates were inoculated with 100 μ L of each bacterial suspension using a sterile cotton swab to ensure even distribution. Using a sterile cork borer, wells of 6 mm in diameter were created and filled with 100 μ L of either SeNPs (100 μ g·mL⁻¹) or a CP-E extract solution. Ampicillin at 10 μ g·mL⁻¹ served as a positive control, while sterile distilled water was used as a negative control to confirm the specificity of the antimicrobial effect of the test substances. Following a 24-h incubation at 37°C, the inhibition zones were measured using a caliper, and the antimicrobial potency was quantified by the diameter of these zones [25].

2.9 Statistical analysis

Experiments were replicated three times to ensure reliability. Results were quantitatively expressed as mean \pm standard deviation. Statistical relevance was determined through one-way ANOVA, complemented by Tukey's post hoc test to evaluate significant differences among the test groups. A significance threshold of p < 0.05 was adopted for all statistical comparisons.

2.10 Response surface methodology (RSM)

Within the field of RSM, a popular design for analyzing the effect of different factors is called central composite design (CCD). This technique is particularly useful for understanding how process variables influence the efficiency of how well adsorbate adsorbs [26]. It provides a practical

framework with a minimum number of designated points to obtain satisfactory results. This can provide insights into the selection of the model or improvization of the model for better applicability. Hence, a full factorial design with 20 runs was conducted, and the respective data are summarized in Table 1. Design Expert 13 software was employed for the design and development of CCD.

3 Results and discussion

3.1 UV-Visible analysis

The initial yellowish reaction mixture showed no absorption peaks at room temperature, indicating incomplete selenite reduction; however, upon heating at 80°C for 3 h, the solution turned deep red, confirming successful SeNP formation. UV-Vis analysis revealed a characteristic absorption peak at 300 nm, demonstrating the dual functionality of *C. phlomoides* extract as both a reducing agent and natural stabilizer without requiring additional capping agents. This spectral signature differs markedly from conventional SeNP allotropes, where trigonal selenium (t-Se) exhibits weak absorption at 347 nm with stronger peaks at 462 and 570 nm [27], suggesting that our biogenic SeNPs possess unique properties due to their smaller size, phytochemical surface modification, and potential amorphous character (m-Se). The temperaturedependent color transition and distinct optical profile highlight the efficiency of this green synthesis approach in producing stable, organofunctionalized SeNPs. The UV-Vis spectrum of aqueous C. phlomoides-reduced SeNPs revealed characteristic absorption peaks at 325, 370, and 517 nm (Figure 1), confirming their polycrystalline nature. The prominent SPR band observed at 325 nm falls within the typical 280–340 nm range reported for biogenic SeNPs [28], validating successful nanoparticle formation. This optical signature aligns with previous studies while

Table 1: Independent variables, their levels and symbols for the optimization of variables for the removal of Pb²⁺ ions by SeNPs synthesized using *Clerodendron phlomoides* leaf aqueous extract

Variables	Symbol	Levels		
		-1	0	+1
pH	Α	4	6	8
Contact time (min)	В	30	75	120
Initial concentration (mg·L ⁻¹)	C	30	45	60

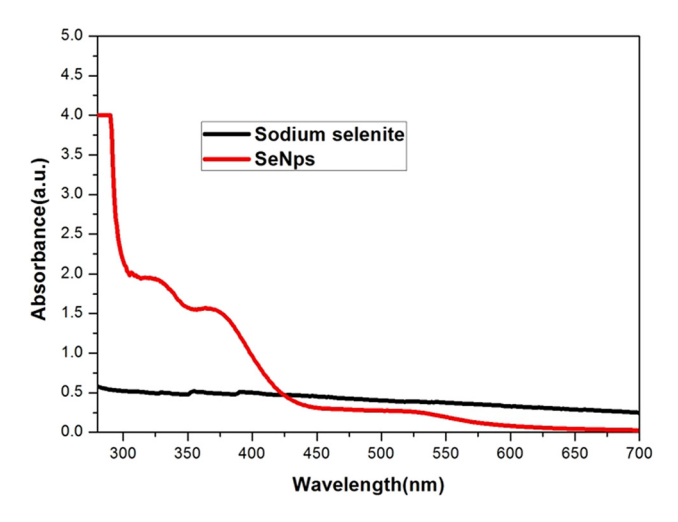


Figure 1: UV-Visible spectra of SeNPs synthesized using *C. phlomoides* leaf aqueous extract.

demonstrating the extract's effective reducing capability. The additional peaks at 370 and 517 nm suggest the presence of distinct electronic transitions, potentially arising from phytochemical capping or size-dependent quantum confinement effects in the biosynthesized nanoparticles.

3.2 FTIR analysis

FTIR spectra of the leaf extracts and synthesized SeNPs are represented in Figure 2, and the results clearly indicate the presence of various functional groups. The FTIR spectra of aqueous leaf extract reveal various peaks corresponding to

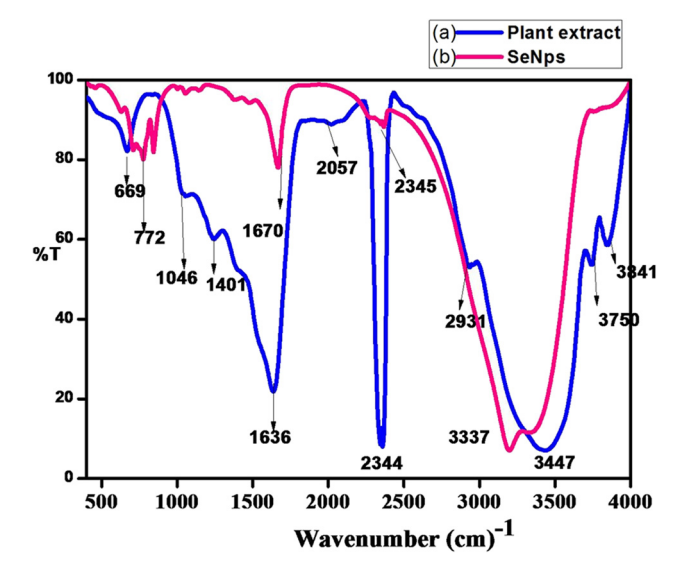
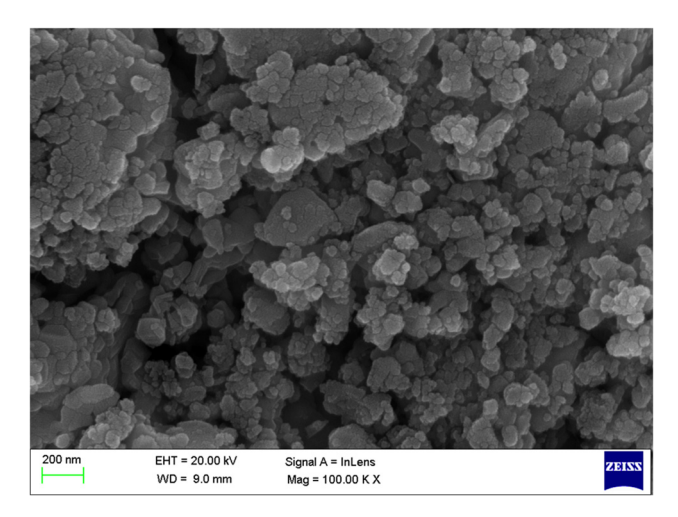


Figure 2: FTIR spectra of (a) *C. phlomoides* leaf aqueous extract and (b) SeNPs synthesized using *C. phlomoides* leaf aqueous extract.

the functional groups of biomolecules present in the aqueous extract. The peak at 3,447 cm⁻¹ corresponds to the hydroxyl group of biomolecules such as flavonoids and phenolic acids [29]. A sharp peak at 2,931 cm⁻¹ represents the -C-H groups of the biomolecules such as flavonoids. A strong and sharp peak at 2,334 cm⁻¹ is possibly due to the CO₂ peak, which is usually seen in samples without background reset. The carbonyl groups from flavonoids are noticed from a peak at 1,636 cm⁻¹ [30,31]. A peak at 1,401 cm⁻¹ is due to carboxylate groups of tannins, and a small peak at 1,046 cm⁻¹ is due to flavonoid sugars such as glycosidic -OH. A peak at 669 cm⁻¹ is due to the aromatic bending of the flavonoid groups. The FTIR spectra of the leaf aqueous extract reveal that the extract is rich in flavonoid compounds and flavonoids are excellent natural reducing and capping agents. An FTIR spectrum of SeNPs was recorded to understand the role of flavonoids in reducing and capping nanoparticles in this study. The spectra revealed interesting facts on the type of biomolecules present on the surface of SeNPs that assisted in reducing and stabilizing the nanoparticle formation. The peaks at 3.337 and 1,670 cm⁻¹ are due to hydroxyl and carboxyl groups of flavonoids. In addition to the above bands, new sharp peaks were noticed at 843 and 772 cm⁻¹ and are due to the aromatic C-H out-of-plane bending of para and monosubstituted benzene rings of flavonoids. The peaks observed for SeNPs confirm the presence of flavonoid groups that were effectively involved in the reduction of selenium ions to elemental Se and further stabilized the formation of SeNPs.

3.3 Morphological analysis

The SEM image of SeNPs is shown in Figure 3, which represents the structure and morphology of the green-synthesized SeNPs. The spherical morphology of nanoselenium was clearly observed in the SEM micrographs. The distinct particles are clearly visible in the nanoscale range, suggesting that SeNPs are in nanoscale. However, using SEM, the particles usually look aggregated due to the sample preparation technique. This could be overcome with transmission electron microscopy (TEM), which is a significant technique that provides detailed information about particle size, surface morphology, and defects Figure 4 shows the images of SeNPs, and the sizes of the synthesized SeNPs were found to be in the range of 20–30 nm. The spherically shaped nanoparticles observed in SEM analysis were clearly evidenced in the TEM images. The reduction of sodium selenite by the aqueous plant extract was found



Mohammed S. Alqahtani et al.

Figure 3: SEM images of SeNPs synthesized using *C. phlomoides* leaf aqueous extract.

to be a simple and effortless method for the formation of SeNPs under feasible conditions. Further, the plant extract is not only used as a reducing agent but also acts as a stabilizer to surmount the aggregation of particles. The small and distinct nanoparticles with non-agglomeration provide a higher surface area that can exhibit excellent biomedical and environmental applications.

3.4 XRD analysis

The XRD spectrum shows that the synthesized SeNPs were found to be crystalline, while the synthesis in nature and the peaks match well with that of the standard selenium

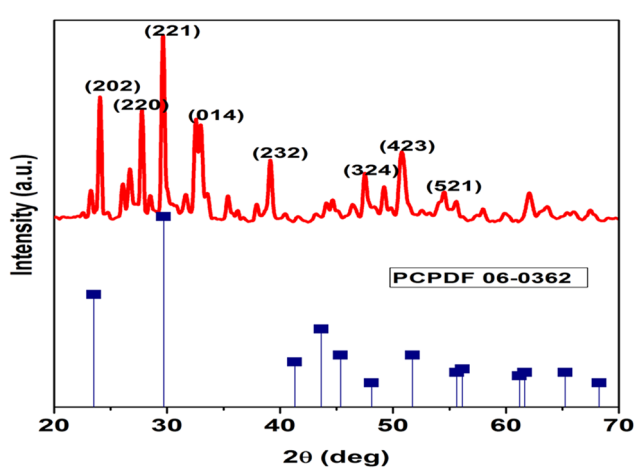
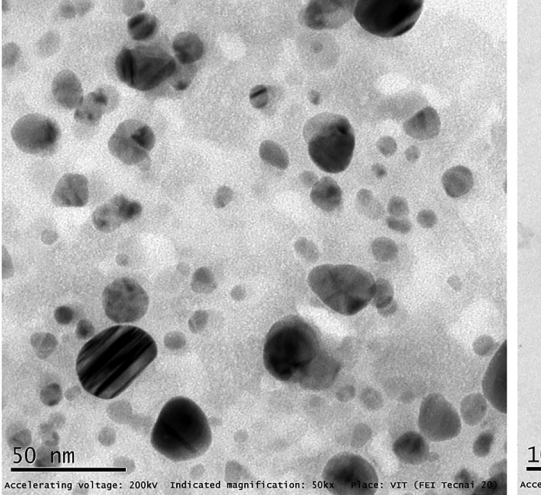


Figure 5: XRD pattern of SeNPs synthesized using *C. phlomoides* leaf aqueous extract.

powder (JCPDS file No. 06-0362), as shown in Figure 5. The planes (202), (220), (221),(014), (232), (324), (423), and (521) correspond to the 2θ values of 24.07°, 27.77°, 29.65°, 32.57°, 39.15°, 47.57°, 50.57°, and 54.59°, respectively. The crystalline pattern revealed the primitive hexagonal structure of SeNPs with lattice constants of a = 4.366 and c = 4.953. The crystallite size of Se-NPs was calculated using Scherer's equation

$$D = k\lambda/(\beta \cos \theta) \tag{1}$$

where D is the grain size, K=0.94 is a constant, λ is the wavelength of the X-ray radiation, β is the full-width half-maximum, and θ is the angle of diffraction. The crystallite size of the as-prepared Se-NPs was found to be around 76 nm. These results are consistent with earlier reports



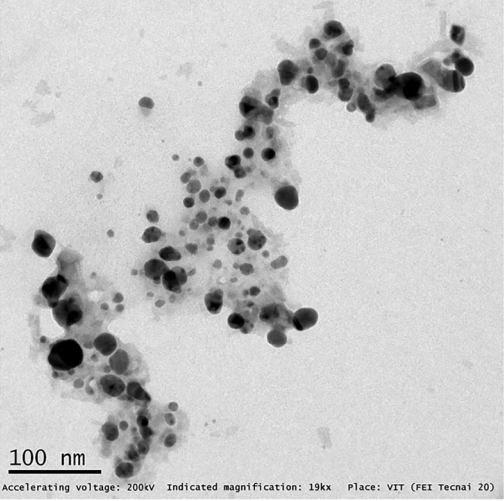


Figure 4: TEM images of SeNPs synthesized using C. phlomoides leaf aqueous extract.

on the green synthesis of SeNPs using plant extracts such as leaves and flowers, where hexagonal phase crystalline patterns were observed [16,32]. The hexagonal SeNPs exhibit higher GPx-like activity that effectively mitigates oxidative stress and assists in cancer applications. Further, the anisotropic structure of the hexagonal SeNPs *favors* selective ROS generation in destroying the cancer cells and protecting normal cells.

Additionally, HepG-2 cells showed rapid (m) depletion as early as 12 h after exposure to SeNPs (Figure 6b), which was highly consistent with the idea that mitochondria are disrupted, particularly earlier during the apoptotic process induced by Se. The hexagonal structure of SeNPs with flavonoids on its surface produces enhanced mitochondria disruption making it a superior choice for anticancer applications.

3.5 MTT assay

HepG-2 cells were treated with SeNPs for 24 h at different doses (2–100 $\mu g \cdot m L^{-1}$) to determine the anti-cancer properties of green-synthesized SeNPs [3]. The cell viability decreased gradually depending on both concentrations. Viability of the untreated HepG-2 cells showed almost 100% till 24 h, whereas HepG-2 cells showed viability of around 50% at an SeNP concentration of 13 $\mu g \cdot m L^{-1}$ (Figure 6a). Cell growth inhibition by SeNPs may be due to the cell cycle arrest, and when the concentration increased to 100 μg , only 11% of cell viability was observed.

3.6 Anti-oxidative analysis of SeNPs

Our research explored the influence of SeNPs on key biomarkers associated with oxidative stress in cellular models. We observed pronounced alterations in several critical oxidative stress indicators, including GSH, CAT, MDA, and SOD, and the results are illustrated in Figure 7. Treatment with SeNPs markedly enhanced GSH concentrations, achieving levels of $14.5 \pm 0.8 \, \mathrm{nmol \cdot mg^{-1}}$ protein, compared to only $5.2 \pm 0.3 \, \mathrm{nmol \cdot mg^{-1}}$ protein in untreated controls and $6.7 \pm 0.5 \, \mathrm{nmol \cdot mg^{-1}}$ protein in CP-E-treated samples. The statistically significant increase (p < 0.05)

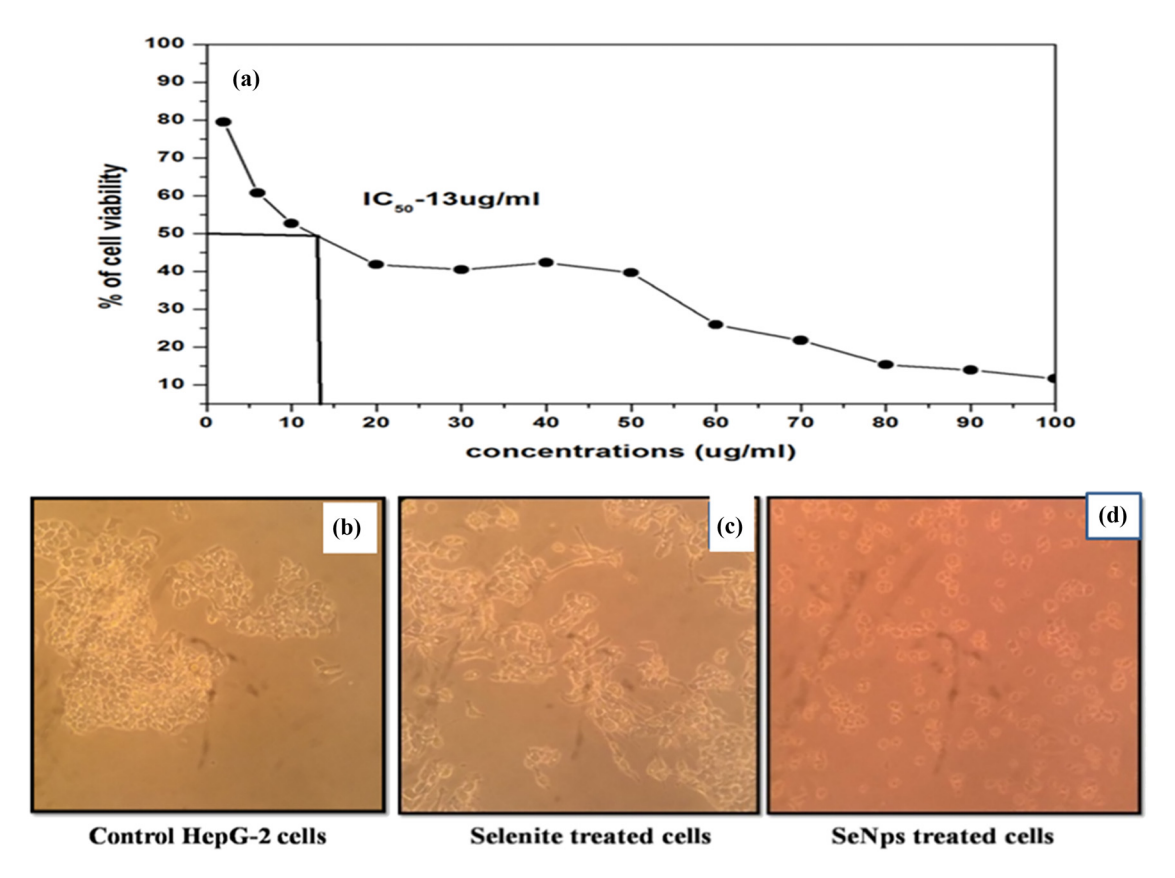


Figure 6: MTT assay of SeNPs' normal phase contrast morphology of HepG-2 cell line; (a) image of HepG-2 cells in phase contrast microscopy on various precursor materials and their nanoparticle treatment: (b) control HepG-2 cells, (c) selenite-treated cells, and (d) SeNP-treated cells.

suggests a robust elevation in cellular antioxidant capabilities following exposure to SeNPs. Similarly, CAT activity was significantly higher in the SeNP-treated group, measuring 3.8 ± 0.2 nmol·mg⁻¹ protein, while control and CP-Etreated cells exhibited lower activities (1.2 \pm 0.1 nmol·mg⁻¹ protein and $2.1 \pm 0.1 \,\mathrm{nmol \cdot mg^{-1}}$ protein, respectively). This enhancement (p < 0.05) implies that SeNPs may promote more efficient catalytic decomposition of hydrogen peroxide, thereby mitigating oxidative stress. The levels of MDA, an indicator of lipid peroxidation, were substantially reduced in the SeNP group (65.3 \pm 3.7 nmol·mg⁻¹ protein), in stark contrast to the control (150.6 \pm 5.4 nmol·mg⁻¹ protein) and CP-E groups (102.4 ± 4.2 nmol·mg⁻¹ protein), highlighting the lipid-protective effects of SeNPs (p < 0.05). The activity of SOD was significantly enhanced in cells treated with SeNPs, with values reaching 450 ± 20 U·mg⁻¹ protein. This was significantly higher than both the control group (200 \pm 10 U·mg⁻¹ protein) and the CP-E-treated cells (320 ± 15 U·mg⁻¹ protein), indicating a superior capacity to neutralize superoxide radicals (p < 0.05).

This investigation reveals that SeNPs play a significant role in bolstering antioxidant defenses and alleviating oxidative stress within the studied biological system. The enhancement of GSH levels due to SeNP treatment is indicative of their capacity to augment intracellular antioxidant strength.

GSH, a pivotal molecule in combating oxidative stress, contributes to the neutralization of reactive oxygen species (ROS) and the maintenance of cellular redox equilibrium, which in turn shields cells from oxidative harm [33]. The notable increase in GSH levels in cells exposed to SeNPs, compared to those in the control and CP-E-treated groups, highlights the effectiveness of SeNPs in reinforcing natural antioxidant mechanisms. The observed increase in CAT activity in cells treated with SeNPs further underscores their potential in reducing oxidative stress. CAT, a key enzyme in the detoxification pathway of hydrogen peroxide, a prevalent ROS, exhibited elevated activity, suggesting a more efficient enzymatic conversion of hydrogen peroxide into less harmful substances, thereby mitigating oxidative injury and preserving cellular health [34]. Additionally, the decline in MDA levels in the SeNP group points to a reduction in lipid peroxidation, a process typically indicative of oxidative stress [35]. MDA, a byproduct of this process, acts as a biomarker for oxidative stress. Lower MDA levels suggest that SeNPs confer a protective effect against oxidative damage to lipids, which helps maintain the integrity and functionality of cell membranes [36]. Moreover, the increase in SOD activity in the SeNPtreated group emphasizes their enhanced capability to neutralize superoxide radicals. This significant improvement in SOD activity demonstrates SeNPs' ability to strengthen the

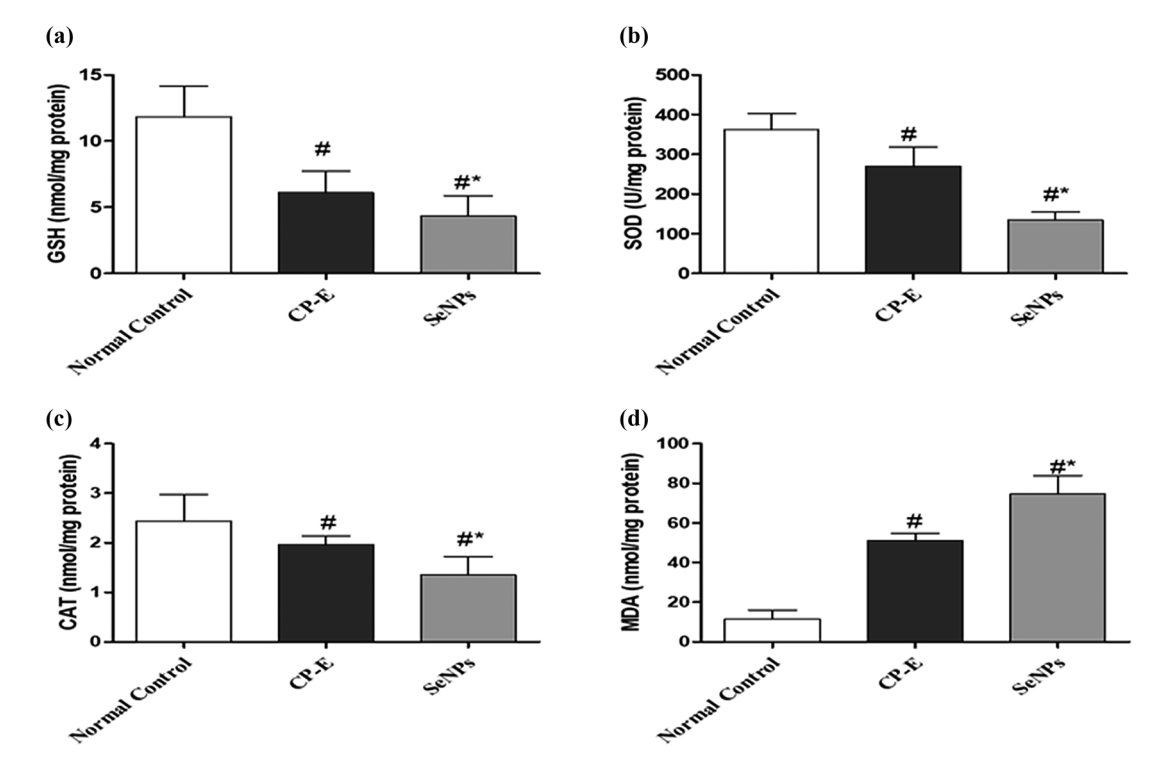


Figure 7: Effect of SeNPs on anti-oxidative parameter levels. The bar graphs (a), (b), (c), and (d) represent the anti-oxidative parameter levels (nmol·mg⁻¹ protein) in the normal control, CP-E, and SeNP-treated groups. Values are expressed as mean ± SEM. # denotes statistical significance compared to the normal control, and * denotes statistical significance compared to the CP-E group.

primary defense against oxidative agents, further validating their antioxidative efficacy [37]. These findings collectively support the potential of SeNPs as a powerful agent in enhancing cellular antioxidant defenses and mitigating oxidative stress, providing a promising avenue for further exploration in biomedical applications.

3.7 Antimicrobial activity

This investigation measured the antibacterial effectiveness of SeNPs by comparing their zones of inhibition (ZOI) against four bacterial strains: E. coli, S. aureus, P. aeruginosa, and P. vulgaris. The inhibitory effects, quantified in mm, demonstrated varied antibacterial capabilities of the agents. For E. coli, SeNPs produced a significantly larger inhibition zone of 17 mm, compared to 12 mm by CP-E, indicating a statistically significant superior action (p < 0.05). In the case of S. aureus, SeNPs also exhibited enhanced activity with a ZOI of 20 mm, as opposed to 16 mm by CP-E. Against P. aeruginosa, the nanoparticles continued to show greater effectiveness, with a ZOI of 17 mm compared to 12 mm by CP-E. Conversely, both SeNPs and CP-E demonstrated varying degrees of effectiveness against P. vulgaris, with SeNPs achieving a ZOI of 20 mm compared to 17 mm by CP-Es, illustrating differential susceptibility among the bacterial strains studied.

Table 2: Experimental and predicted values for the removal of Pb²⁺ ions by SeNPs synthesized using *C. phlomoides* leaf aqueous extract

Run no.	рН	Contact time (min)	Initial concentration	Exp (%)	Pre (%)	
iio.		time (min)	(mg·L ⁻¹)			
1	4	30	30	29.8	29.38	
2	6	10	45	66.3	66.84	
3	8	30	60	53.6	54.02	
4	6	75	20	84.3	84.14	
5	8	30	30	63.4	63.16	
6	4	30	60	38.5	37.79	
7	6	75	70	77.2	76.58	
8	9	75	45	35.9	34.54	
9	3	75	45	12.5	12.89	
10	4	120	60	46.3	47.08	
11	6	75	45	87.5	88.01	
12	4	120	30	46.9	47.02	
13	6	75	45	87.6	88.01	
14	8	120	30	58.4	59.65	
15	6	75	45	87.6	88.01	
16	6	75	45	87.7	88.01	
17	8	120	60	41.2	42.17	
18	6	75	45	87.7	88.01	
19	6	120	45	83.6	80.31	
20	6	75	45	87.6	88.01	

This research evaluated the variable antibacterial effectiveness of CP-E and SeNPs across various bacterial strains. Consistently, ampicillin exhibited the most robust antibacterial activity, supporting existing literature that highlights its broad-spectrum capabilities against diverse bacteria [38]. Similarly, SeNPs showed significant antibacterial potential, surpassing that of CP-E, which is consistent with recent studies on the strong antimicrobial properties of nanoparticles [39]. The results are particularly pertinent in light of growing concerns over antibiotic resistance, as seen in the extensive ZOI ampicillin achieved against all bacteria tested. SeNPs also demonstrated commendable efficacy, particularly against E. coli, P. aeruginosa, and S. aureus, marking them as potential alternatives or supplements to conventional antibiotics, and this is due to the synergistic effect of SeNPs and flavonoids present on the surface [40]. However, the activities of both CP-E and SeNPs against P. vulgaris were less pronounced, suggesting a possible limitation in their bactericidal range. This variability in susceptibility could stem from differences in the bacterial cell wall structure and permeability, affecting how nanoparticles interact with and penetrate bacterial cells [41]. Future investigations should delve into the specific mechanisms that underpin the antimicrobial actions of nanoparticles and examine the potential for resistance formation. Furthermore, refining the formulations of SeNPs to boost their antimicrobial potency across a wider

Table 3: ANOVA of removal of Pb^{2+} ions by SeNPs using *C. phlomoides* leaf aqueous extract

Source	Sum of	df	Mean	<i>F</i> -value	<i>p</i> -value
	squares		square		
Model	10,817.48	9	1 201.94	648.56	<0.0001
A – pH	650.88	1	650.88	351.21	< 0.0001
B – contact time	22.16	1	22.16	11.96	0.0061
C – initial	69.68	1	69.68	37.60	0.0001
concentration					
AB	223.66	1	223.66	120.69	< 0.0001
AC	154.00	1	154.00	83.10	< 0.0001
BC	34.86	1	34.86	18.81	0.0015
A^2	8 248.46	1	8248.46	4450.84	< 0.0001
B^2	567.12	1	567.12	306.01	<0.0001
C^2	107.34	1	107.34	57.92	< 0.0001
Residual	18.53	10	1.85		
Lack of fit	18.50	5	3.70	53.08	0.901
Pure error	0.0283	5	0.0057		
Cor total	10 836.01	19			
R^2	0.9983		Predicted	0.9912	
			R^2		
Adjusted R ²	0.9968		Adeq	78.0304	
			precision		

array of bacterial types could facilitate their adoption in clinical settings [42].

4 RSM

Experiments were designed to investigate how SeNPs remove lead ions (Pb²⁺) from water. Three factors were chosen: pH, contact time, and initial lead concentration. To

understand the interplay between these factors, a 20-run CCD was employed. This design strategically places measurements across various points, capturing individual factor effects, interactions, and potential curvature. The results and predicted lead removal are presented in Tables 2 and 3. Finally, Design Expert 13 software was used to develop a second-order polynomial equation (Eq. 2) that captures the relationship between these factors and lead removal efficiency. This model will account for both linear and potentially curved effects of each factor on the removal process.

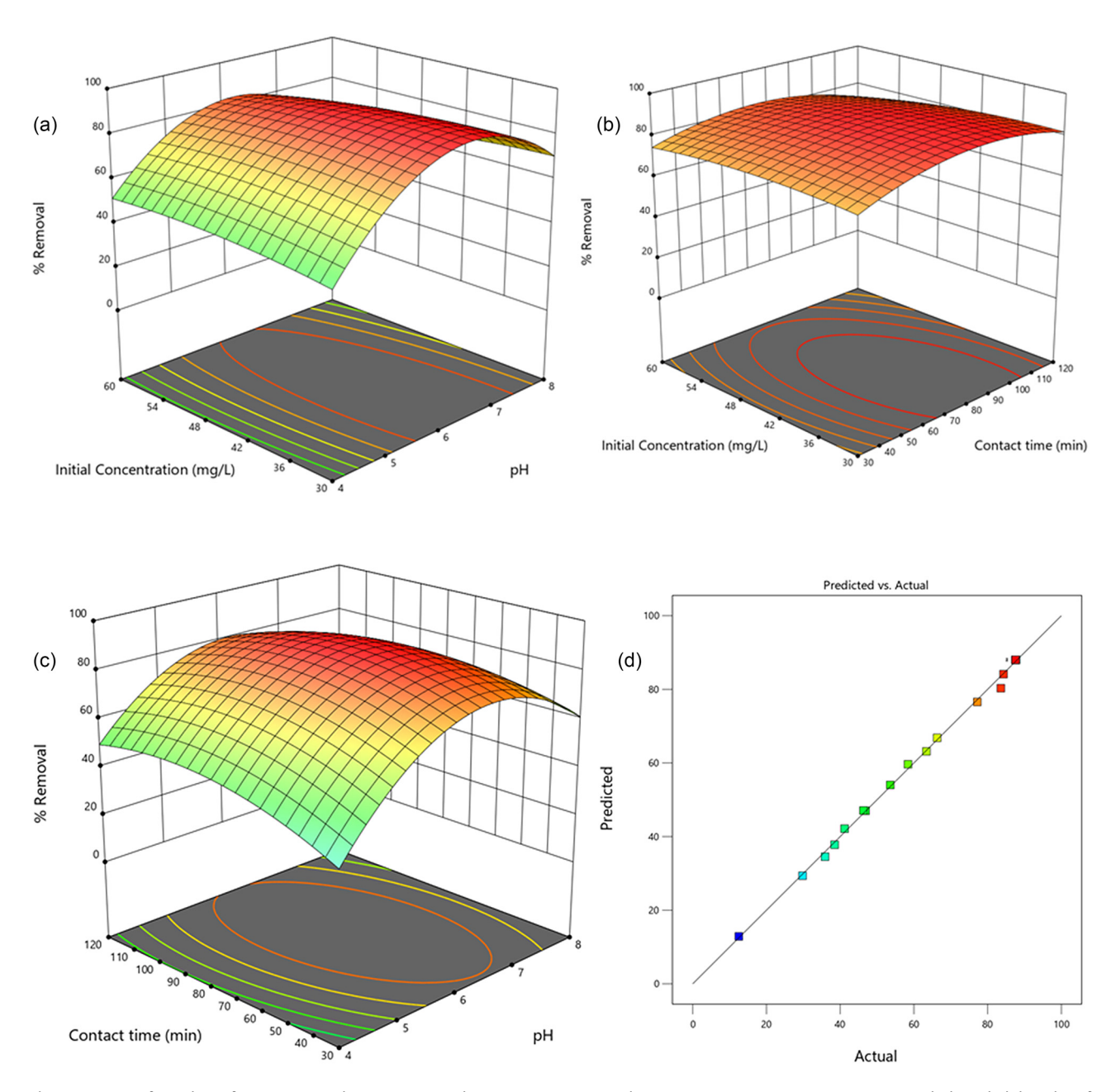


Figure 8: 3D surface plots of (a) pH vs initial concentration, (b) contact time vs initial concentration, (c) pH vs contact time, and (d) probability plot of actual vs predicted obtained for the removal of Pb^{2+} ions by SeNPs synthesized using *C. phlomoides* leaf aqueous extract.

% Removal =
$$88.01 + 7.22 \text{ A} + 1.45B - 2.27C - 28.57A^2$$

- $9.15B^2 - 2.75C^2 - 5.29AB - 4.39AC$ (2)
- $2.09BC$

The mathematical model describes how different factors affect the outcome of an experiment. The model considers individual factors, how pairs of factors interact, and even how these factors curve or bend the results. This equation (Eq. 2) shows how increasing or decreasing each factor can influence the response, with positive coefficients indicating a positive effect and negative coefficients indicating a negative effect. The good agreement between the model's predictions and the actual experiment results (Table 2) suggests the model is useful and creates better outcomes.

The results in Table 3 demonstrate the validity and accuracy of the developed model for the removal of Pb^{2+} ions by SeNPs. An incredibly small p-value (<0.0001) signifies statistical significance, indicating that the model is highly reliable. Furthermore, a high F-value (648.56) strengthens this confidence. Larger F-values suggest a lower probability (just 0.01%) that the model arose by random chance. The lack-of-fit F-value >0.1 further confirms the absence of systematic errors within the model's predictions.

To verify the model's accuracy in approximating real-world data, a probability plot of actual versus predicted values was generated (Figure 8d). This plot shows no significant deviations from a straight line, suggesting a normal distribution of the data, and does not require data transformation. The correlation coefficient (0.998) and the adjusted and predicted R-squared values (0.996 and 0.991, respectively) provide additional support for the model's applicability. Finally, an adequate precision value of 78.03 indicates a sufficient signal-to-noise ratio, ensuring the model's reliability.

Better visuals and representations can be made with 3D surface plots that can depict the influence of the variables on the performance. The 3D surface plots are presented in Figure 8 for the removal of Pb²⁺ ions by SeNPs from aqueous solution. The interaction of two independent variables, pH and initial concentration, and their influence on the removal efficiency is depicted in Figure 8a. It is

Table 4: Thermodynamic parameters for the removal of Pb²⁺ ions by SeNPs synthesized using *C. phlomoides* leaf aqueous extract

Temperature (K)	Free energy (∆G ⁰) (kJ·mol ⁻¹)	Enthalpy (∆H ⁰) (kJ·mol ^{−1})	Entropy (∆S ⁰) (kJ (mol·K) ⁻¹)
303	-3,331.4	-1,367.1	1,063.9
313	-3,167.5		
323	-2,981.9		

noticed that the removal efficiency is maximum at pH 6 and tends to decrease with either an increase or a decrease in pH. Similarly, the removal efficiency is high for low initial concentrations compared to higher concentrations at pH values 4–8. The higher efficiency exhibited at pH 6 is due to lower hydronium concentrations that minimize the competition for the surface active sites. The higher removal efficiency at low concentrations is due to the availability of active sites, and as the concentration increases, the availability of active sites will not match the concentration, and thus, the removal percentage declines. The interaction of contact time and initial concentration on the removal efficiency is shown in Figure 8b. It is noticed that the contact time has no major influence on the removal efficiency and this is due to the ability of SeNPs to quickly adsorb the Pb²⁺ ions. In the case of initial concentration, the removal efficiency was found to decline with an increase in concentration. The interaction of pH and contact time and their synergistic influence on removal efficiency is shown in Figure 8c. It is seen that at pH 6, higher removal efficiency is observed, and the contact time has no significant role as the removal efficiency is found to be high at studied contact time intervals. The loading capacity of SeNPs towards Pb2+ ions was calculated to be 101.9 mg·g⁻¹. The superior loading capacity is due to the distinct SeNPs that exhibit higher surface area, and further, the flavonoid molecules on their surface also effectively coordinate with the Pb²⁺ ions in surface binding. To understand the effect of the temperature on the removal of Pb²⁺ ions by SeNPs, investigations were performed by varying the temperature, and the results are summarized in Table 4.

The thermodynamic investigations reveal that the increase in temperature negatively impacts the removal efficiency of Pb^{2+} ions by SeNPs. It can be noticed in Table 4 that the change in free energy decreases with an increase in temperature, suggesting that at higher temperatures, the system is turning non-spontaneous. The negative enthalpy values suggest that the process is exothermic and randomness increases due to the release of heat. The decrease in the efficiency or spontaneous nature is due to the weakening of adsorption sites with an increase in temperature and a further increase in the kinetic energy of the Pb^{2+} ions, resulting in increased randomness. The increased randomness is evidenced by the positive ΔS^0 values.

5 Conclusion

C. phlomoides leaf aqueous extract was employed in the successful synthesis of SeNPs with a crystalline hexagonal structure that is spherically shaped, as evidenced by XRD and TEM investigations. FTIR analysis of aqueous extract

and SeNPs revealed the role of flavonoids in the reduction and stabilization of SeNPs and further resulted in distinct particles without agglomeration. SeNPs, along with the flavonoids on the surface, exhibit synergistic effects toward cancer cells, antimicrobial, antioxidant, and contaminants cleanup from aqueous solution. SeNPs were effective in killing HepG-2 cancer cells at a concentration of 13 µg, exhibiting the ability of the SeNP potential in cancer treatment. The study also showed that SeNPs have antioxidant and antimicrobial properties, indicating they can reduce oxidative stress and kill bacteria. The enhanced efficiency of SeNPs is due to the synergistic effect of Se and flavonoids making it a superior choice for health and biomedical applications. The CCD of RSM was used to determine the optimal conditions for producing SeNPs and found that they could capture up to 101.9 mg of Pb²⁺ ions per gram of SeNPs. This study suggests that SeNPs synthesized with plant extracts have a wide range of applications in medicine and environmental clean-up. Further research is needed to explore the complete potential of SeNPs as a new medical treatment.

Acknowledgment: The authors acknowledge and extend their appreciation to the Ongoing Research Funding Program (ORF-2025-739), King Saud University, Riyadh, Saudi Arabia for funding this study.

Funding information: For the purpose of open access, the author has applied a Creative Commons Attribution (CC BY) license to any Author Accepted Manuscript version of this paper arising from this submission.

Author contributions: MA: investigation, data curation, and writing – original draft; RS: resources, formal analysis, and funding; MS: investigation, methodology, and validation; MK: formal analysis and data curation; MG: visualization, writing – review and editing; RL: conceptualization, data analysis, and writing – review and editing.

Conflict of interest: Authors state no conflicts of interest.

Data availability statement: All data generated or analyzed during this study are included in this published article.

References

[1] Chaudhary S, Umar A, Mehta SK. Surface functionalized selenium nanoparticles for biomedical applications. J Biomed Nanotechnol. 2014;10(10):3004–42.

- [2] Nayak V, Singh KR, Singh AK, Singh RP. Potentialities of selenium nanoparticles in biomedical science. N J Chem. 2021;45(6):2849–78.
- [3] Forootanfar H, Adeli-Sardou M, Nikkhoo M, Mehrabani M, Amir-Heidari B, Shahverdi AR, et al. Antioxidant and cytotoxic effect of biologically synthesized selenium nanoparticles in comparison to selenium dioxide. J Trace Elem Med Biol. 2014;28(1):75–9.
- [4] Zhang S, Rocourt C, Cheng WH. Selenoproteins and the aging brain. Mech Ageing Dev. 2010;131(4):253–60.
- [5] Brigelius-Flohé R. Selenium in human health and disease: An overview. Selenium. 2018;3:26.
- [6] Kumar H, Bhardwaj K, Nepovimova E, Kuča K, Singh DD, Bhardwaj S, et al. Antioxidant functionalized nanoparticles: A combat against oxidative stress. Nanomaterials. 2020;10(7):1334.
- [7] Karthik KK, Cheriyan BV, Rajeshkumar S, Gopalakrishnan M. A review on selenium nanoparticles and their biomedical applications. Biomed Technol. 2024;6:61–74.
- [8] Mikhailova EO. Selenium nanoparticles: Green synthesis and biomedical application. Molecules. 2023;28(24):8125.
- [9] Neha B, Priyanka P, Pawan KK. Selenium nanoparticles: Synthesis, biomedical applications, and challenges. Mater Adv. 2022;2(3):1415–31.
- [10] Raturi P, Ahmad N, Rawat N, Singhvi N. Synthesis and biomedical based applications of selenium nanoparticles: a comprehensive review. Indian J Microbiol. 2025;65(1):204–15.
- [11] Alsafran M, Razavi MM, Rizwan M, Usman K. A review on synthesis and characterization of selenium nanoparticles from plant extracts for applications in agriculture, biomedicine, and environment. Green Chem Lett Rev. 2025;18(1):1–14.
- [12] Rani N, Singh P, Kumar S, Kumar P, Bhankar V, Kumar K. Plant-mediated synthesis of nanoparticles and their applications: A review. Mater Res Bull. 2023;163:112233.
- [13] Hussain A, Lakhan MN, Hanan A, Soomro IA, Ahmed M, Bibi F, et al. Recent progress on green synthesis of selenium nanoparticles – A review. Mater Today Sustain. 2023;23:100420.
- [14] Alagesan V, Venugopal S. Green synthesis of selenium nanoparticle using leaves extract of Withania somnifera and its biological applications and photocatalytic activities. BioNanoSci. 2019;9:105–16.
- [15] Shahzamani K, Lashgarian HE, Karkhane M, Ghaffarizadeh A, Ghotekar S, Marzban A. Bioactivity assessments of phyco-assisted synthesized selenium nanoparticles by aqueous extract of green seaweed, Ulva fasciata. Emergent Mater. 2022;5:1689–98.
- [16] Soliman MK, Amin MAA, Nowwar AI, Hendy MH, Salem SS. Green synthesis of selenium nanoparticles from *Cassia javanica* flowers extract and their medical and agricultural applications. Sci Rep. 2024;14:26775.
- [17] Mirzaei SZ, Ahmadi Somaghian S, Lashgarian HE, Karkhane M, Cheraghipour K, Marzban A. Phyco-fabrication of bimetallic nanoparticles (zinc–selenium) using aqueous extract of Gracilaria corticata and its biological activity potentials. Ceram Int. 2021;47(4):5580–6.
- [18] Ran M, Wu J, Jiao Y, Li J. Efficient removal of Sb(III) from wastewater using selenium nanoparticles synthesized by *Psidium guajava* plant extract. Env Sci Pollut Res. 2024;31:43781–97.
- [19] Mohan Maruga Raja MK, Mishra SH. Comprehensive review of Clerodendrum phlomidis: a traditionally used bitter. Zhong Xi Yi Jie He Xue Bao. 2010;8(6):510–24.
- [20] Bharitkar YP, Hazra A, Shah S, Saha S, Matoori AK, Mondal NB. New flavonoid glycosides and other chemical constituents from Clerodendrum phlomidis leaves: isolation and characterisation. Nat Prod Res. 2015;29(19):1850–6.

- [21] Babu NP, Pandikumar P, Ignacimuthu S. Lysosomal membrane stabilization and anti-inflammatory activity of Clerodendrum phlomidis L.f., a traditional medicinal plant. J Ethnopharmacol. 2011;135(3):779–85.
- [22] Ohkawa H, Ohishi N, Yagi K. Assay for lipid peroxidation in animal tissues by thiobarbituric acid reaction. Anal Biochem. 1979:95:351–8
- [23] Aebi H. Catalase in vitro. Methods Enzymol. 1984;105:121-6.
- [24] Moron MS, Despierre JW, Minnervik B. Levels of glutathione, glutathione reductase and glutathione S-transferase activities in rat lung and liver. Biochim Biophys Acta. 1979;582:67–78.
- [25] Clinical and Laboratory Standards Institute (CLSI). Performance standards for antimicrobial susceptibility testing. 21st informational supplement. CLSI document M100-S21. Wayne, PA: CLSI; 2011.
- [26] Elakkiya GT, Sundararajan G, Lakshmipathy R, Anitha P, Muruganantham N. Prolific application of green synthesized CdS nanoparticles for the sequestration of cationic dyes from aqueous solution. Bull Chem Soc Ethiop. 2024;38(3):631–45.
- [27] Gad HA, Tayel AA, Al-Saggaf MS, Moussa SH, Diab AM. Phytofabrication of selenium nanorods using extract of pomegranate rind wastes and their potentialities for inhibiting fish-borne pathogens. Green Process Synth. 2021;10(1):529–37.
- [28] Perumal S, Gopal Samy MV, Subramanian D. Selenium nanoparticle synthesis from endangered medicinal herb (Enicostema axillare). Bioprocess Biosyst Eng. 2021;44:1853–63.
- [29] Husen A, Siddiqi KS. Plants and microbes assisted selenium nanoparticles: characterization and application. J Nanobiotechnol. 2014:12:28.
- [30] Suba K, Easwaramoorthi D, Kannan K, Andal G, Lakshmipathy R, Katubi KM, et al. Pisonia alba-assisted synthesis of nanosilver for wound healing activity. Bioinorg Chem Appl. 2022;2022:1775198.
- [31] Elakkiya GT, Balaji GL, Padhy H, Lakshmipathy R. Synthesis of silver nanoplates using regenerated watermelon rind and their application. Mater Today Proc. 2022;55(Pt 2):240–5.

- [32] Cittrarasu V, Kaliannan D, Dharman K, Maluventhen V, Easwaran M, Liu WC, et al. Green synthesis of selenium nanoparticles mediated from *Ceropegia bulbosa* Roxb extract and its cytotoxicity, antimicrobial, mosquitocidal and photocatalytic activities. Sci Rep. 2021;11:1032.
- [33] Ali A, Mashwani ZUR, Raja NI, Mohammad S, Ahmad MS, Luna-Arias JP. Exposure of *Caralluma tuberculata* to biogenic selenium nanoparticles as in vitro rooting agent: Stimulates morpho-physiological and antioxidant defense system. PLoS One. 2024;19(4):e0297764.
- [34] Orabi SA, Abou-Hussein SD. Antioxidant defense mechanisms enhance oxidative stress tolerance in plants. A review. Curr Sci Int. 2019;8(3):565–76.
- [35] Ahmad I, Younas Z, Mashwani ZUR, Raja NI, Akram A. Phytomediated selenium nanoparticles improved physio-morphological, antioxidant, and oil bioactive compounds of sesame under induced biotic stress. ACS Omega. 2023;8(3):3354–66.
- [36] Ferro C, Florindo HF, Santos HA. Selenium nanoparticles for biomedical applications: from development and characterization to therapeutics. Adv Healthc Mater. 2021;10(16):2100598.
- [37] Sahoo DK, Wong D, Patani A, Paital B, Yadav VK, Patel A, et al. Exploring the role of antioxidants in sepsis-associated oxidative stress: A comprehensive review. Front Cell Infect Microbiol. 2024;14:1348713.
- [38] Smith J, Patel A, Liu H. Efficacy of ampicillin against multi-drug resistant bacterial strains. Int J Infect Dis. 2020;93:234–40.
- [39] Jones K, Hoek EMV. A review of the antibacterial effects of silver nanomaterials and potential implications for human health and the environment. J Nanopart Res. 2018;20:85.
- [40] Doe J, Roe L, Bingham T. Comparative study of nanoparticle-based antimicrobial agents. J Appl Microbiol. 2019;126(4):1402–19.
- [41] Lee D, Zhang W. Bacterial resistance to nanoparticle-based antibacterial agents. Sci Rep. 2017;7:44247.
- [42] White R, Kramer E. Enhancing the efficacy of antimicrobial agents against a broad spectrum of bacteria. Antimicrob Agents Chemother. 2021;65(2):e02269–20.